T · H · E
OHIO
STATE
UNIVERSITY

Simulations of Radar Scattering Over a Rough Sea Surface

Khalid Jamil and Robert J. Burkholder

The Ohio State University

ElectroScience Laboratory

Department of Electrical Engineering
1320 Kinnear Road
Columbus, Ohio 43212

20040604 115

5027272-101

REPORT DOCUMENTATION PAGE	1. REPORT NO.	2.	3. Recipient's Accession No.	
4. Title and Subtitle Simulations of Radar Scattering over a Rough Sea Surface			**5. Report Date** March 2004	
			6.	
7. Author(s) Khalid Jamil and Robert J. Burkholder			**8. Performing Org. Rept. No.** 743971-1	
9. Performing Organization Name and Address **The Ohio State University** **ElectroScience Laboratory** **1320 Kinnear Road** **Columbus, OH 43212**			**10. Project/Task/Work Unit No.**	
			11. Contract (C) or Grant (G) No. (C) N00014-03-1-0128	
12. Sponsoring Organization Name and Address Office of Naval Research Program Officer: James King Ballston Center Tower One 800 N. Quincy Street Arlington, VA 2217-5600			**13. Report Type/Period Covered** Final Report	
			14.	
15. Supplementary Notes				

16. Abstract (Limit: 200 words)

Forward scattering from a 2D rough sea surface is simulated using the Generalized Forward-Backward (GFB) method in a Monte Carlo fashion. Measurements were performed using a scaled ocean model in the NSWC Carderock Maneuvering and Sea-Keeping (MASK) wavetank facility. The mean, standard deviation and probability density function (PDF) of the computational and experimental data is compared and good agreement is found. Backscattering from a floating target on the rough sea surface is also computed. Results of a new hybrid approach are presented for computing the backscatter from a target on a rough sea surface by decoupling the target from the surface.

17. Document Analysis

a. Descriptors Sea surface, Electromagnetic scattering, Rough surfaces, Radar cross sections, Numerical analysis, Monte Carlo method, Integral equations, Physical optics, Reciprocity, radar measurements.

b. Identifiers/Open-Ended Terms

c. COSATI Field/Group

18. Availability Statement	**19. Security Class (This report)** Unclassified	**21. No. of Pages** 48
	20. Security Class (This page) Unclassified	**22. Price**

(See ANSI-Z39.18)	*See Instructions on Reverse*	**OPTIONAL FORM 272(4-77)** Department of Commerce

Acknowledgements

Table of Contents

List of Figures

List of Tables

Chapter 1

Introduction

Over the past several years, computer and analytic models have been developed to simulate and compute the radar cross-section RCS of a target over the rough sea surface [1-3]. Recently, scattering measurements have been conducted in the NSWC Carderock Maneuvering and Sea Keeping (MASK) facility. MASK is an indoor wave tank capable of generating scaled ocean surfaces as a function of sea state. This report describes the computer simulation of forward and backscattering measurements performed inside the MASK facility and tries to investigate any differences between the two. Some initial simulation results from the previous year are reported in [4].

The MASK wave maker creates a rough sea surface for the desired wave spectrum for a given sea state. The sea state dictates the wave height and wavelength for a given wind speed. Two kinds of measurements are performed: Forward-scatter and backscatter. In forward-scatter measurements, a transmitting antenna is used to illuminate the rough sea surface and a receiving antenna is placed at various heights to measure the sea-scattered field. For backscatter measurements, a target is suspended over the waves, or placed floating on the rough sea surface. The experimental setup for both the cases is shown in Figure 1.1. The measurements encompass a variety of sea states and antenna heights. Each measurement is performed over a range of frequencies for a significant period of time to collect enough statistical samples. The results are plotted in the form of a probability density function (PDF) of the scattered power. The frequencies, wave spectrum and physical dimensions are 1/10th scale to simulate an L-band radar over a realistic ocean using an X-band measurement system. The scaling and experimental setup is discussed in more detail in Chapter 2. Three measurement sets, namely SS000, SS001 and SS002 are provided to validate the computational simulations. These sets are for sea states 0, 3, and 5, respectively, horizontal polarization, with waves generated by the "short bank" wave maker.

1
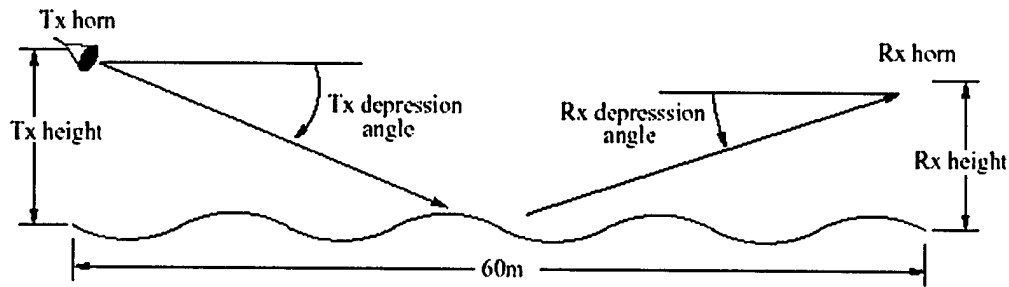
(a) Forward scatter experimental set-up.
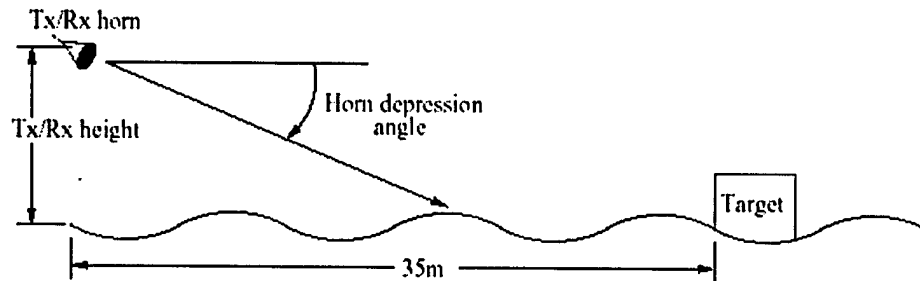
(b) Backscatter experimental set-up

Figure 1.1: Experimental set-up for forward and backscatter measurements over a rough sea surface.

The measurements are simulated using the spectrally accelerated generalized forward-backward method (SAGFB) [1,7,8,14]. Chapter 3 compares the Monte Carlo computational predictions with the measurements. Good agreement is found between the two PDFs along with some differences. Effort is made to investigate into the differences. Still some differences are found unresolved and are left as future work of this project. The PDF behavior of forward scatter simulations is also investigated and it is found that the numeric PDF obtained from statistical data fits perfectly with Rician PDF, at least for horizontal polarization and low grazing angle cases. This helps better understanding the scattering mechanism from the rough sea surface and reducing the number of simulations required to obtain the converged results. At the end, Chapter 3 also presents a few cases of forward scattering for vertical polarization and long bank waves.

Chapter 4 presents the simulation results for backscatter experiments. In [4] a suspended rotating plate was simulated. In this report, we present simulations for a floating Styrofoam cylinder target. These are the first simulations of a target that truly free-floats on the waves. Previous simulations of floating targets allowed targets to move up and down with the waves, but not roll. It is found that the floating effect is very significant for RCS predictions over rough surfaces. It must be noted that free-floating is modeled in

2

this report and no considerations are made to target weight distribution or inertial/buoyancy properties. However, in this case, the measurement data has not provided to date. Therefore, no comparisons are made. It is planned as a future part of the project.

Chapter 5 discusses a novel approach to decouple the scattering the large sea surface from that of the target using a reciprocity formulation. Hybrid techniques can then be applied for efficient computation of each problem. The main advantage of this new technique is to reduce the computational domain significantly for RCS computations. The formulation is exact and for 3D targets. However, an approximation is made to find the surface currents over the target. Initial results are presented for 2D targets and horizontal polarization. Results for 3D targets and other polarizations are planned as part of the continuing effort.

1.1 Generalized Forward-Backward Method

The GFB method is used here to obtain most of the numerical solutions. The GFB method [14] was developed for two-dimensional geometries involving a target on or above a very long rough surface, as illustrated in Figure 1.2. It is a numerically rigorous method of moments (MoM) solution that is solved iteratively by taking advantage of the forward and backward nature of the propagation over a long rough surface. The forward-backward iteration makes the solution converge only in a few cycles. The GFB is a generalization of the forward-backward (FB) method [5] or equivalently, the method of ordered multiple interactions [6], which were developed for single-valued rough surfaces without a target present. The GFB method isolates the portion of the MoM matrix associated with the target region and solves it directly within the forward-backward iteration process. Figure 1.2 shows the matrix decomposition used in the GFB solution. The efficiency of the GFB method is remarkably improved by adapting the spectral acceleration approach of [7]. This work is described in [1] and [8].

The only limitation of the GFB method is its restriction to 2D geometries. Also, note that the infinite sea surface must be artificially truncated to apply the MoM solution. To reduce the effects of the endpoint truncation, tapered R-card material is attached to both ends of the sea surface as described in [8]. Comparison with infinite surface reference solutions shows that this approach provides excellent accuracy. The simulations reported in this report are obtained with the FB and GFB methods.

Source

Region 1 MoM Region 3 S

Region 2

$\overline{\overline{Z}}^{sq}$

$\overline{\overline{Z}}^{pq}$

$\overline{\overline{Z}}\cdot\overline{I}=\overline{V} \quad \Leftrightarrow$

$\overline{\overline{Z}}^{lq}$

$\cdot \quad |\overline{I}| \quad = \quad |\overline{V}|$
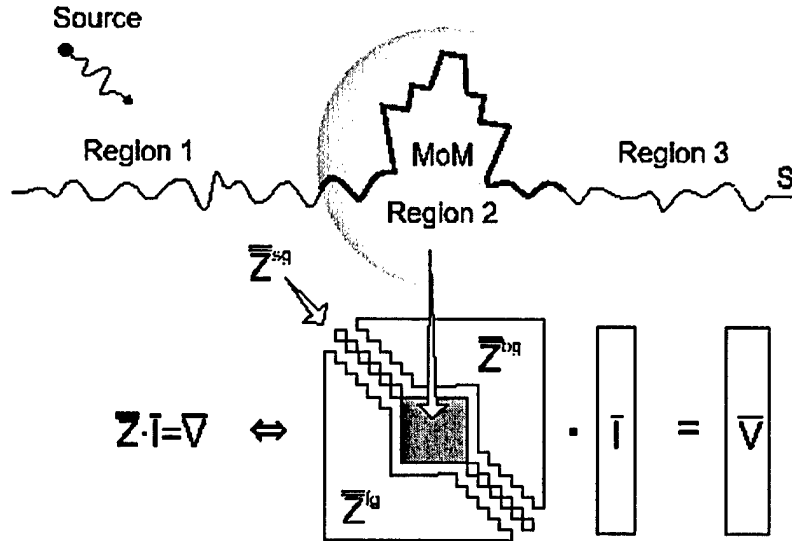
Figure 1.2: Matrix decomposition used in the generalized forward-backward method. The region 2 matrix is solved directly within the forward-backward iteration process.

1.2   Organization of Report

Chapter 2 describes the experimental setup and parameters used in the NSWC Carderock MASK facility, as well as descriptions of the hydrodynamics and material modeling used in the simulations. The plots naming conventions and Monte Carlo statistical processing is also discussed. Chapter 3 presents the results for forward scattering simulations and compares them to the measurements for horizontal polarization. Some simulation results are also presented for vertical polarization and long bank cases. Chapter 4 presents the simulation results for backscatter from a floating/non-floating cylindrical PEC target. Chapter 5 describes a new approach to solve the scattering problem by decoupling the sea scattering from that of the target using reciprocity theorem. Conclusions are discussed in Chapter 6.

Chapter 2

Experimental Setup

2.1   Forward Scatter Measurements

In the forward scatter measurements, the experimental setup is as shown in Figure 1.1(a). A transmitting antenna is used to illuminate the sea surface and a receiving antenna is used to measure the incident plus scattered power from the surface. The horizontal range from the transmitter to the receiver is 60m. Both antennas are of the same polarization. The transmitter antenna is fixed at a height of 5.25m with depression angle of $-9.9°$. The receiving antenna is placed at three different heights: 0.75m, 1.25m and 1.75m with depression angle set to $-3°$.

The transmit (Tx) and receive (Rx) horn antennas are identical corrugated conical horn antennas with aperture diameter 0.146m and flare angle approximately $25°$. The half-power beamwidth is approximately $20°$. The transmitter and receiver position naming conventions along with their heights and depression angles are given in Table 2.1.

	Transmitter			Receiver		
	Position	Height (m)	Dep. angle	Position	Height (m)	Dep. angle
1	A	1.05	$-2.0°$	A	0.75	$-3°$
2	B	3.14	$-6.0°$	B	1.25	$-3°$
3	C	5.25	$-9.9°$	C	1.75	$-3°$

Table 2.1: Vertical positions and orientations of the horn antennas for the forward-scattering measurements.

The received signal is measured from 8 to 12 GHz for sea state 0, 3 and 5 as generated in the NSWC Carderock MASK facility. The measurements are designed to simulate the scattering over rough ocean surface in L-band (0.8 to 1.2 GHz) frequency range. So, the frequency is scaled up by a factor of 10 and the physical dimensions and wave spectrum are scaled down by 1/10 in the MASK facility. The water depth is 20 ft.

In the measurements, 128 frequency steps are used for the frequency range 8-12 GHz, whereas 21 steps are used in the simulations to save computational time. 3000 samples are collected in the measurements for each horn position, sampled at a rate of 10 Hz for 300 seconds on a time-evolving surface. 500 samples corresponding to 500 randomly generated rough surfaces are generated in the simulations.

Simulation set SS000 is for sea state 0, i.e., no roughness and is used for reference and calibration purposes. Simulation set SS001 is for sea state 3 and SS002 for sea state 5. The relationship between sea state, wave height and wave spectrum is discussed in Section 2.3.

2.2   Backscatter Measurements

The backscattering experimental set-up is shown in Figure 1.2(b). A transmit/receive horizontally polarized horn antenna is placed at position B (3.14m high with -6° depression angle). It illuminates the target at a range of 29.3m over the rough sea surface. The target in this case is a circular cylinder made out of styrofoam wrapped with conductive film, 12 inches high and 17 inches in diameter. Sea states 3 and 5 are investigated. A rotating plate target has also been simulated, as reported in [4], although a complete simulation set is awaiting a *request for simulation* from the sponsor.

Two cases are considered in the simulations: free-floating and non-floating target. A floating target rolls with the waves and is assumed to have zero inertia. The weight distribution or buoyancy effects are not modeled. A non-floating target is fixed over the waves without any rolling. In each case, 512 samples are computed in a Monte Carlo run using random rough sea surfaces generated by Pierson-Moskowitz spectrum.

2.3   Hydrodynamics

The rough sea surface is generated in the MASK facility with a wave maker that produces an approximate Pierson-Moskowitz ocean spectrum [9]. The spectrum is appropriately modified to simulate an ocean surface at 1/10 scale for various sea states. Figure 2.1 plots the actual measured wave spectra for scaled simulations of sea state 3 and 5. As the figure shows, the spectra have similar characteristics as of Pierson-Moskowitz i.e., a higher sea state gives rise to larger, longer ocean waves. The measured spectra are given as a function of the angular frequency ω of the ocean waves, which is related to wavenumber K by the dispersion relation $\omega = \sqrt{gK}$, where $g = 9.81$m/s is the gravitational acceleration constant at sea level [10].

Table 2.2 gives the sea states as a function of wind speed and wave height of the ocean surfaces simulated in the measurements, where $H_{1/3}$ is the average *significant wave height* for each sea state [10]. The RMS wave height is approximately one-third of $H_{1/3}$. Table 2.2 also states the average scaled RMS wave heights and the actual measured RMS wave

heights. It is seen that the measured wave heights are slightly lower than expected for each sea state.
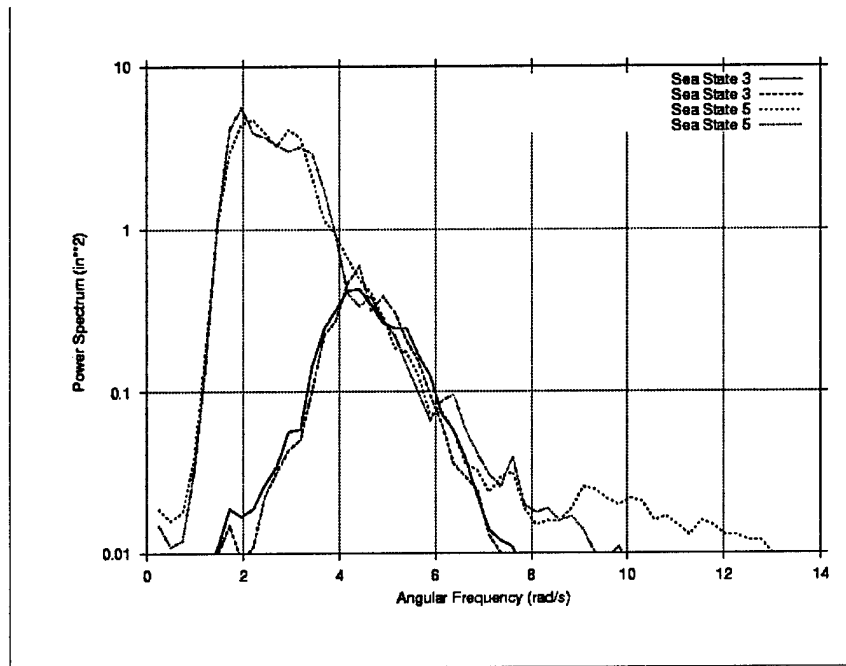
Figure 2.1: Experimental sea spectra for 1/10 scale Pierson-Moskowitz ocean simulations.

Sea state	Wind speed (m/s)	$H_{1/3}$	$1/10\ H_{1/3}$	Measured RMS	1/10 RMS
3	6.53	0.87	0.087	0.023	0.029
5	11.59	3.25	0.325	0.074	0.108

Table 2.2: Wave heights for sea states 3 and 5 (in meters). $H_{1/3}$ is the average significant wave height for each sea state.

The computer simulations use a pure Pierson-Moskowitz ocean spectrum adjusted to give the same RMS wave height as the measurements. In the simulations, the ocean surface is also scaled by a factor 1/10 with respect to the full scale spectrum.

2.4 Material Characterization of Sea Water

The dielectric permittivity ε and magnetic permeability μ of the sea water are given by

$$\varepsilon = (\varepsilon' - j\varepsilon'')\varepsilon_o - j\frac{\sigma_c}{\omega}$$

$$\mu = \mu_o$$

(2.1)

where $\mu_o = 4\pi \times 10^{-7}$ h/m and $\varepsilon_o = 8.854 \times 10^{-12}$ f/m are the permeability and permittivity of free space, respectively, $\sigma_c = 4$ mho/m is the conductivity of sea water, and ω is the radian frequency of the time-harmonic electromagnetic field. At a frequency of 10 GHz and temperature $25°$ C, $\varepsilon = (55 - j37)\varepsilon_o$, which are the parameters used here in the computer simulations. While the water in the MASK tank does not have as high salinity as sea water, it is expected to have a comparable conductivity due to other dissolved minerals in the water.

The surface integral equation approach used here models the sea surface as an impenetrable impedance surface with surface impedance given by,

$$Z_s = \sqrt{\frac{\mu_o}{\varepsilon}}$$

(2.2)

For such a high dielectric constant and loss tangent, the impenetrable surface impedance model is very accurate for all angles of incidence in the 8-12 GHz frequency band.

2.5   Statistical Processing

As scattering from a rough sea surface is a probabilistic phenomenon, each forward or backward scattering case is run for 500 random ocean surfaces. The surfaces are not time-evolving but generated in Monte Carlo fashion using random seeds. The probability density function (PDF) of the scattered power as a function of frequency is of interest here. To generate the PDF from statistical data, the range between the maximum and minimum scattered power (in dBs) is divided into 50 bins. The numeric PDF is obtained by computing the probability of each sample occurrence and normalizing the area under the probability curve such that,

$$\int_0^1 x\,P(x)\,dx = 1$$

(2.3)

where $P(x)$ is the probability of sample x. In Chapter 3, it is shown that the numeric PDF obtained from forward scattering over rough sea surface is identical to Rician PDF given as,

$$PDF(|\widetilde{E}|) = \frac{|\widetilde{E}|}{\sigma^2}\exp\left(-\frac{|\widetilde{E}|^2 + \mu^2}{2\sigma^2}\right)I_o\left(\frac{|\widetilde{E}|\mu}{\sigma^2}\right)$$

(2.4)

8

where σ is the standard deviation and μ is the mean of the coherent power. $I_o(.)$ is the modified Bessel function of zero order. Note that this PDF is for the magnitude of the normalized field $|E|$ so it may be plotted on the same dB scale as the coherent and incoherent power. It may be shown this PDF becomes Gaussian for $|\widetilde{E}|\mu/\sigma^2 \gg 1$ case.

A Rician PDF is normally used where the received signal has the form of signal plus noise [12].

The frequency scale in the plots is divided into 21 linear steps. Convergence tests show that 500 samples are enough to obtain a good PDF of the statistical data. However, it is found in Chapter 3 that statistical parameters like mean and standard deviation converge much faster than a full PDF curve. This finding is of computational importance because in that case, the PDF for a certain case can be obtained from lesser samples using a standard known PDF such as Rician with faster-converged mean and standard deviation of the data.

Chapter 3

Forward Scattering Simulations

The forward scattering experimental set-up is shown in Figure 3.1. A transmitting horn antenna at a fixed height of 5.25m illuminates the rough sea surface. A receiving horn antenna measures the forward scattered energy at three different positions 0.75m, 1.25m and 1.75m. The transmitting and receiving horn antennas are set at depression angles of -9.9 and -3 degrees respectively. Two different sea states, 3 and 5, are studied while sea state 0 is used as a reference. The received field normalized to the incident field is computed in the computer simulations, and is defined by

$$\tilde{E} = \frac{E^i + E^s}{E^i} \tag{3.1}$$

where E^i and E^s are the free-space incident and backscattered fields, respectively. The 2D forward-backward method is used to simulate the forward scatter measurements. 500 samples are computed for each simulation in a Monte Carlo fashion and probability density function (PDF) is plotted against the frequency range 8-12 GHz.
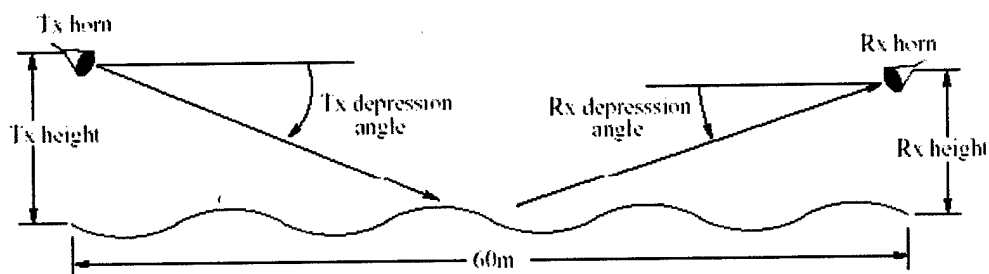
Figure 3.1: Experimental setup for forward scatter measurements over rough sea surface.

3.1 Simulation Set 000 (SS000)

The simulation setup is the same as experimental setup, shown in Figure 3.2. Sea state 0 i.e., flat surface case, is simulated here. The transmitter is placed at 5.5m with –9.9° depression angle while the receiver is at three different heights (0.75m, 1.25m, 1.75m) with –3° depression angle. Both antennas are horizontally polarized and 60m apart. Figure 3.3 (a) to (c) shows the forward scatter over a flat sea surface computed by the GFB code and compares it to the analytical solution by finding the incident and reflected fields via geometrical optics. The sea-reflected field is modified by plane wave reflection coefficient for sea water given by

$$R_h(\theta^i) = \frac{Z_s \cos\theta^i - 1}{Z_s \cos\theta^i + 1} \tag{3.2}$$

where R_h is reflection coefficient for horizontal polarization, θ^i is the incidence angle measured from surface normal and Z_s being the surface impedance of sea water.
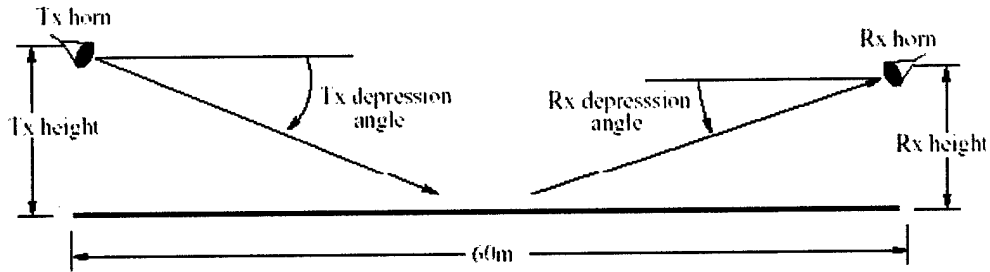
Figure 3.2: Experimental setup for forward scatter measurements over flat sea surface.
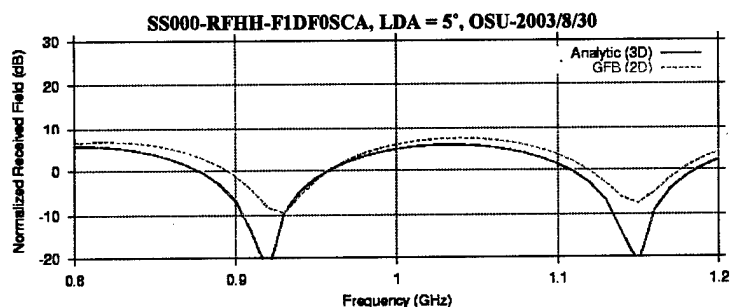
(a) Receiver at position A (height = 0.75m).
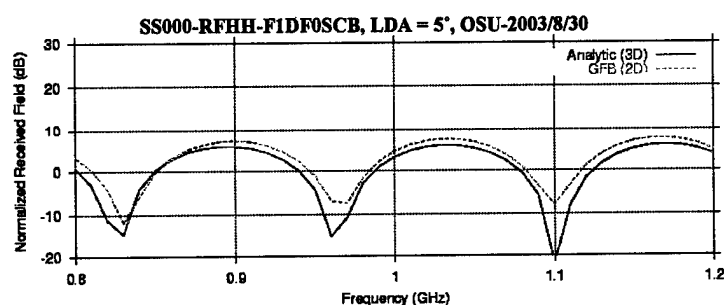
(b) Receiver at position B (height = 1.25m).
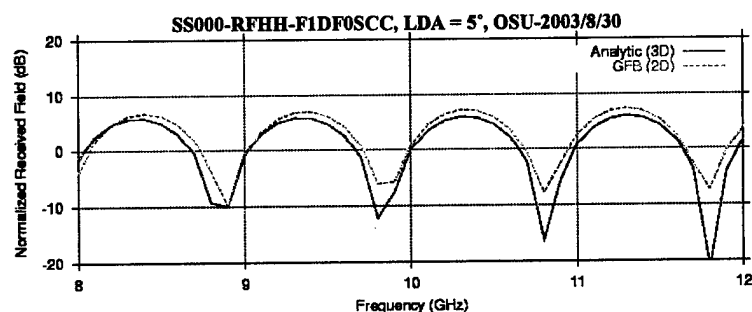
(c) Receiver at position C (height = 1.75m).

Test	FwdSct
Data Set	F1DF3SC(A,B,C)
Run Name	SS000
Polarization	HH
Sea State	0
Range	60m
Transmitter	-9.9° @ 5.25m
Receiver	-3° @ (0.75,1.25,1.75m)
LDA	5^0
Samples	500
PDF Bins	30
Organization	OSU
Date	2003/8/30

Figure 3.3: Comparison of forward scatter from flat sea surface (sea state 0) between GFB computation and analytical solution (geometrical optics).

3.2   Simulation Set 001 (SS001)

The basic setup for computation is the same as shown in Figure 3.1. The transmitter is located at a height of 5.25m with a depression angle of –9.9 degrees. The receiver is placed at three different heights of 0.75m, 1.25m and 1.75m with a depression angle of – 3 degrees. Both antennas are 60m apart and horizontally polarized. Sea state 3 is used to compute 500 samples and the statistical data is processed to compute the mean, standard deviation and numerical probability density function. Figure 3.2 to 3.4 shows the forward scatter numeric PDF plotted against frequencies 8 – 12 GHz. Sea state 0 (flat surface case) is also plotted for reference. The PDF plots show the relative spread in the Monte Carlo data around the mean.

Test	FwdSct
Data Set	F1DF3SCA
Run Name	SS001
Polarization	HH
Sea State	3
Range	60m
Transmitter	-9.9^0 @ 5.25m
Receiver	-3^0 @ 0.75m
LDA	5^0
Samples	500
PDF Bins	30
Organization	OSU
Date	2004/1/6

Figure 3.4: Forward scatter probability density function (PDF) for sea state 3, horizontal polarization, Tx height = 5.25m, Rx height = 0.75m.

13

Figure 3.5: Forward scatter probability density function (PDF) for sea state 3, horizontal polarization, Tx height = 5.25m, Rx height = 1.25m.

Test	FwdSct
Data Set	F1DF3SCB
Run Name	SS001
Polarization	HH
Sea State	3
Range	60m
Transmitter	-9.9^0 @ 5.25m
Receiver	-3^0 @ 1.25m
LDA	50
Samples	500
PDF Bins	30
Organization	OSU
Date	2004/1/6

Figure 3.6: Forward scatter probability density function (PDF) for sea state 3, horizontal polarization, Tx height = 5.25m, Rx height = 1.75m.

Test	FwdSct
Data Set	F1DF3SCC
Run Name	SS001
Polarization	HH
Sea State	3
Range	60m
Transmitter	-9.9^0 @ 5.25m
Receiver	-3^0 @ 1.75m
LDA	5^0
Samples	500
PDF Bins	30
Organization	OSU
Date	2004/1/6

14

3.3   Simulation Set 002 (SS002)

The simulation setup is the same as shown in Figure 3.1. A transmitter is located at a height of 5.25m with depression angle set to –9.9 degrees while the receiver is placed at 0.75m, 1.25m and 1.75m consecutively in Figures 3.7, 3.8 and 3.9, respectively, with depression angle set to –3 degrees. Both antennas are horizontally polarized and 60m apart. In this case, sea state 5 is used to compute 500 samples in a Monte Carlo simulation. The data is processed statistically and numerical probability density function (PDF) is plotted against frequencies 8 – 12 GHz. The mean gain, mean gain ± one standard deviation σ and sea state 0 (flat surface) case are also included for reference. The PDF plots show that the forward scattering is highly incoherent for sea state 5, because the interference pattern between the incident and sea scattered fields is no longer visible as in the sea state 3 results.

Test	FwdSct
Data Set	F1DF5SCA
Run Name	SS002
Polarization	HH
Sea State	5
Range	60m
Transmitter	-9.9^0 @ 5.25m
Receiver	-3^0 @ 0.75m
LDA	5^0
Samples	500
PDF Bins	30
Organization	OSU
Date	2004/1/6

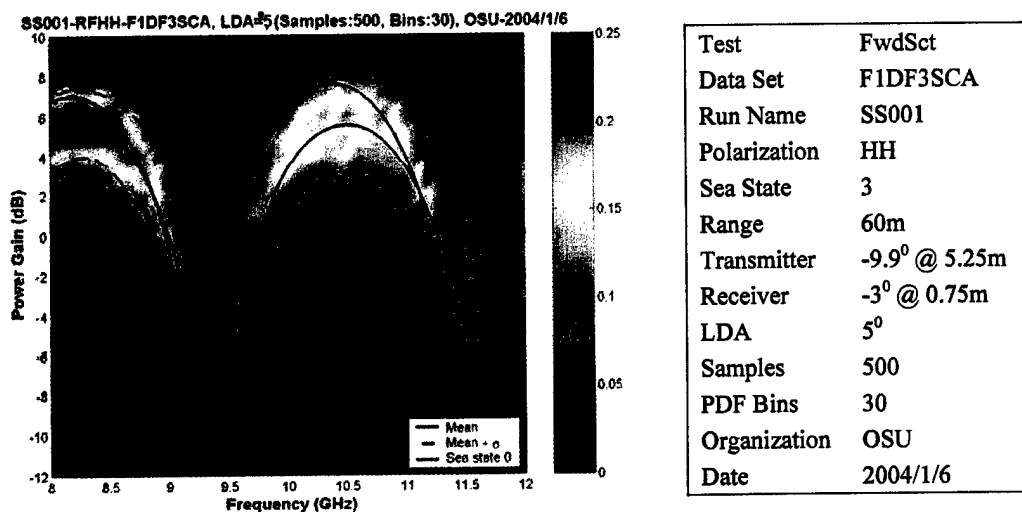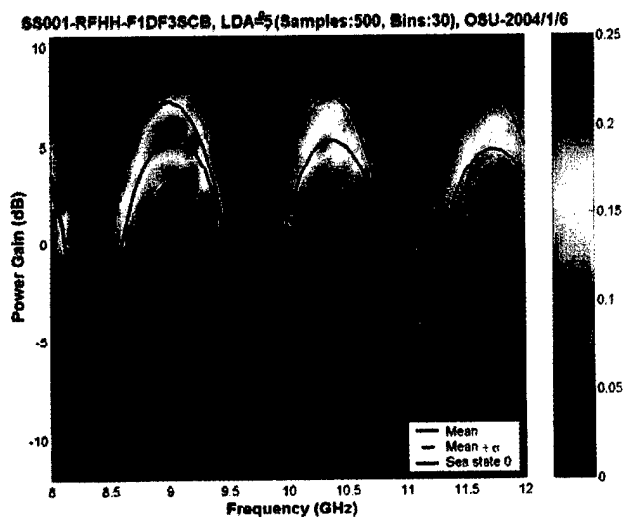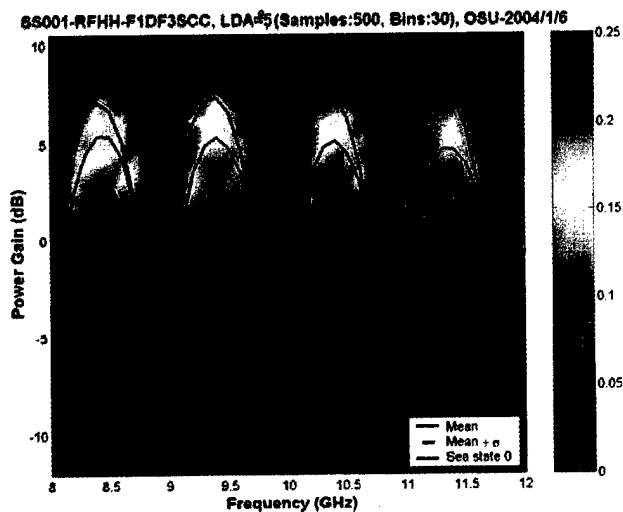**Figure 3.7:** Forward scatter probability density function (PDF) for sea state 5, horizontal polarization, Tx height = 5.25m, Rx height = 0.75m.

SS002-RFHH-F1DF5SCB, LDA:5(Samples:500, Bins:30), OSU-2004/1/6

Test	FwdSct
Data Set	F1DF5SCB
Run Name	SS002
Polarization	HH
Sea State	5
Range	60m
Transmitter	-9.9^0 @ 5.25m
Receiver	-3^0 @ 1.25m
LDA	5^0
Samples	500
PDF Bins	30
Organization	OSU
Date	2004/1/6

Figure 3.8: Forward scatter probability density function (PDF) for sea state 5, horizontal polarization, Tx height = 5.25m, Rx height = 1.25m.

SS002-RFHH-F1DF5SCC, LDA:5(Samples:500, Bins:30), OSU-2004/1/6

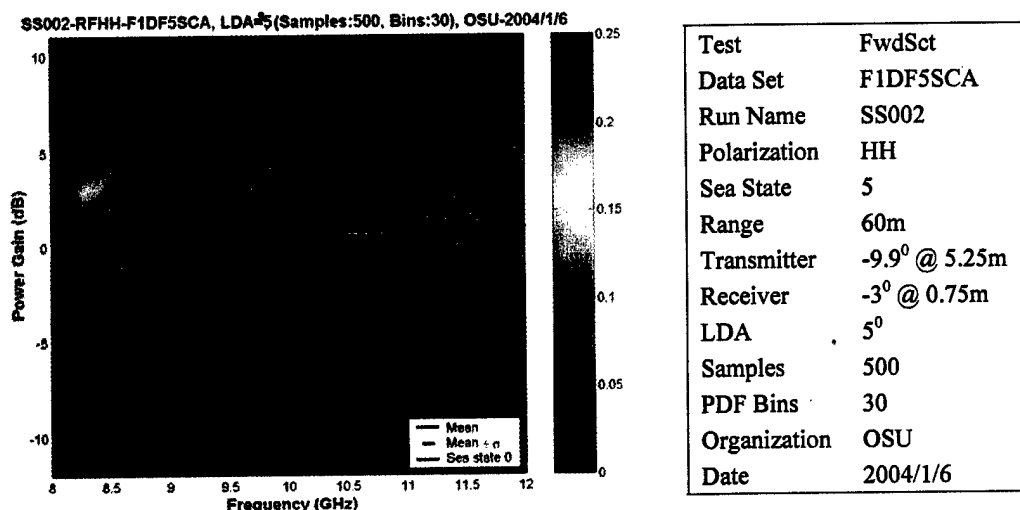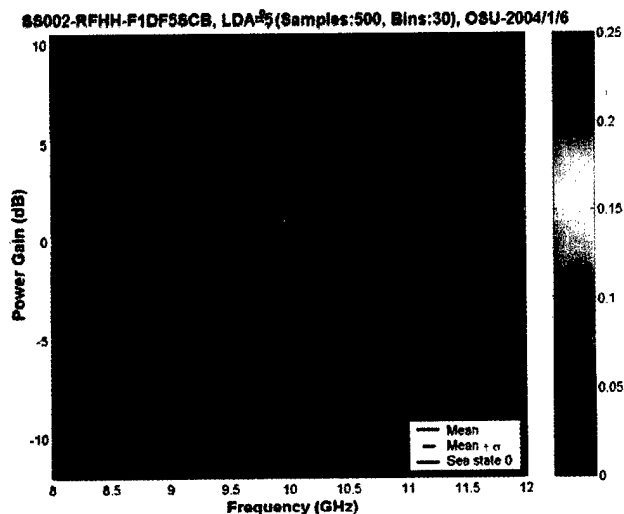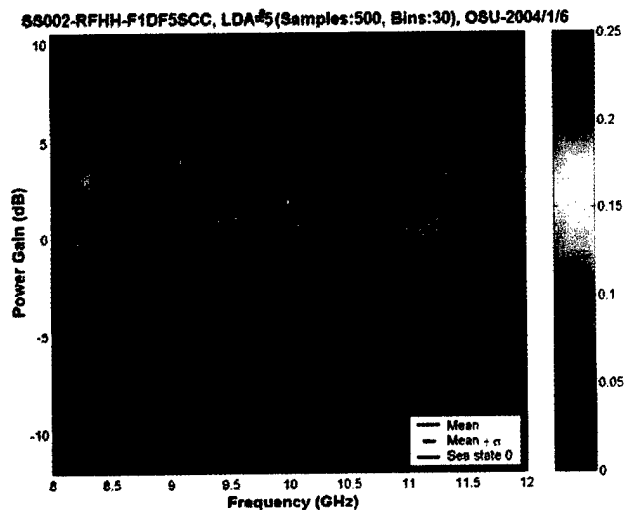| Test	FwdSct
Data Set	F1DF5SCC
Run Name	SS002
Polarization	HH
Sea State	5
Range	60m
Transmitter	-9.9^0 @ 5.25m
Receiver	-3^0 @ 1.75m
LDA	5^0
Samples	500
PDF Bins	30
Organization	OSU
Date	2004/1/6

Figure 3.9: Forward scatter probability density function (PDF) for sea state 5, horizontal polarization, Tx height = 5.25m, Rx height = 1.75m.

16

3.4 Comparing Numeric PDF to Rice PDF

Figure 3.10 shows the numeric PDF (green line) for the simulation set 001 case (forward scattering, sea state 3, Tx = -9.9^0 @ 5.25m, Rx = -3^0 @ 0.75m, horizontal polarization) at 10 GHz for 500 samples. The mean and standard deviation is computed from the numeric data and used to plot the Rice PDF (blue line). Close agreement is found between the numeric and Rician PDFs (computed on a magnitude scale and plotted on dB scale). Similar investigation is done at other frequencies and sea states. It is concluded that the forward scatter data from rough sea surface exhibits Rician PDF behavior. Figure 3.11 compares the Numeric PDF with the Rice PDF for the same case as above for frequencies 8-12GHz. (It is noted that the PDFs in Figure 3.11 are computed from the magnitude of the signal, rather than the dB value, so the plots appear slightly different than Figure 3.4.)
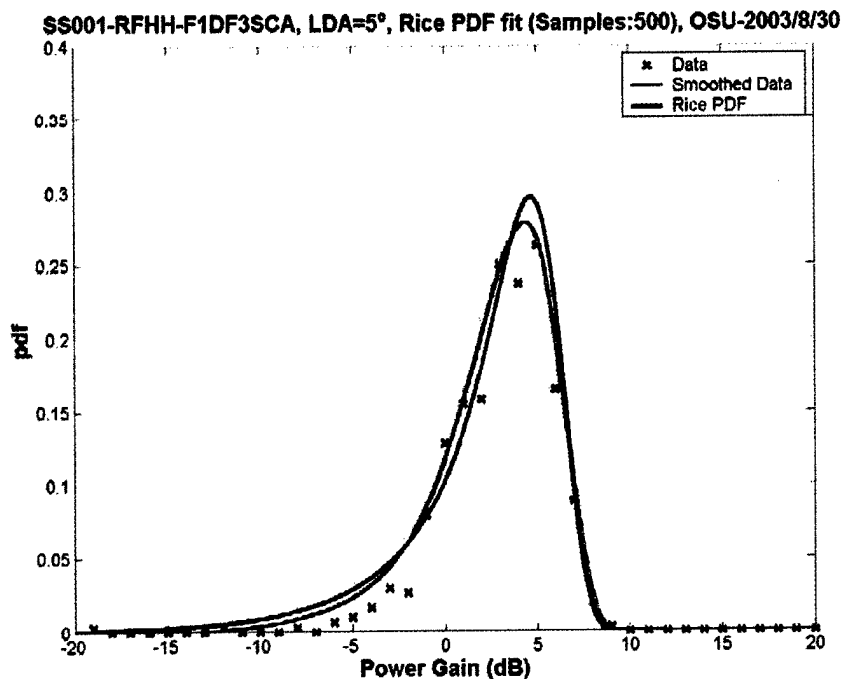

Figure 3.10: Comparison between numeric PDF and Rice PDF for forward scatter simulation from rough sea surface.
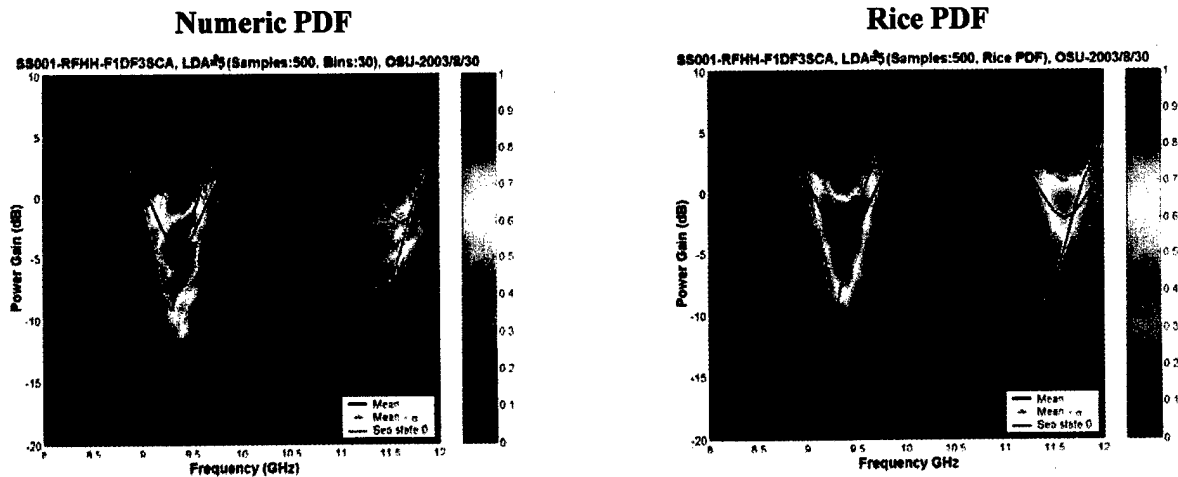
Numeric PDF   **Rice PDF**

Figure 3.11: Comparison between numeric PDF and Rice PDF for forward scatter simulation from rough sea surface.

3.5   Simulations vs. Measurements

The initial simulations sets SS001 and SS002 were submitted to Jerry Smith of NSWC-Carderock for review. He then responded with a *modeling review package* with the processed measured data, as well as his comments on the simulations vs. measurements. These results are presented here.

Figures 3.12 and 3.13 compare the GFB computed PDFs with the measured ones from the MASK facility for Simulation Set SS001 (sea state 3) and Simulation Set SS002 (sea state 5) respectively. The configuration is the same as shown in Figure 3.1. The following observations are made from comparison.

- Overall, a good agreement is found between the measured and computed PDF.
- The measured sea state 0 response agrees well with the predicted one (solid blue line in each of the plots).
- A slight difference in frequencies is found where the interference pattern peaks and nulls are occurring.
- In the measurements, the mean interference pattern is showing a downward trend with increase in frequency. In the simulations this downward trend with increasing frequency is present in some cases, but is less noticeable.
- The computed standard deviation is slightly smaller than the measured one in some cases.
- The predicted data is more spread out around the mean than the measured. There is more red and orange around the mean in the measurements.

18

Simulation Set SS001

Figure 3.12: Comparison between simulation and measurements for Simulation Set SS001 forward scatter simulation from rough sea surface.

Simulation Set SS002

GFB Simulation

MASK Measurement

Figure 3.13: Comparison between simulation and measurements for Simulation Set SS002 for forward scatter simulation from rough sea surface.

3.6 Hydro Spectrum Comparison

To begin to investigate the differences between the GFB computations and measurements, the measured hydro spectrum of the water waves is used to generate the random surfaces in the GFB code instead of the Pierson-Moskowitz spectrum. Figure 3.14 compares the two spectra, and 3.15 compares the GFB computed results. As Figure 3.15 shows, there is very little difference in the PDFs, so the difference in the hydro spectra does not explain the differences between the computed and measured PDFs.
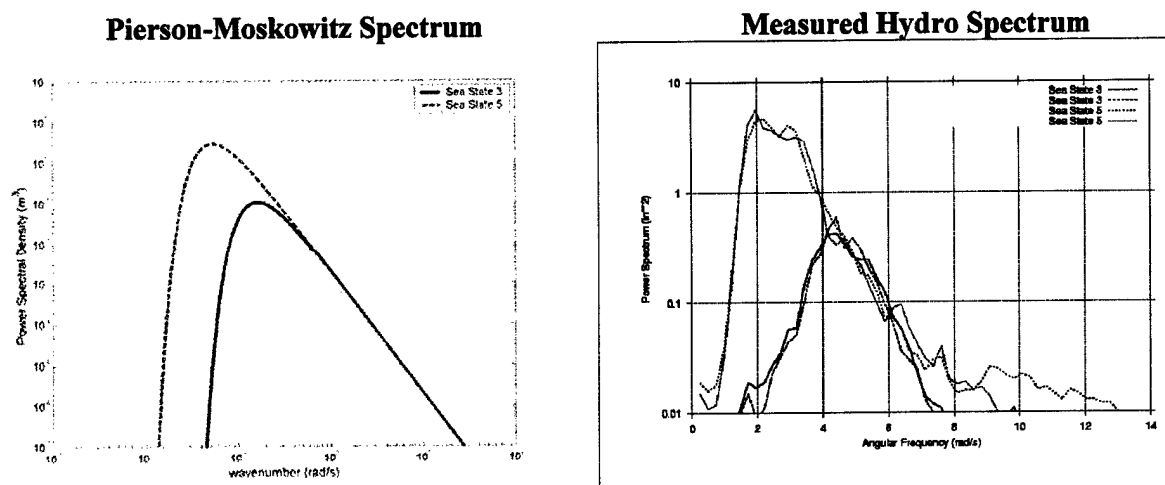
Figure 3.14: Comparison between Pierson-Moskowitz and measured hydro spectrum.

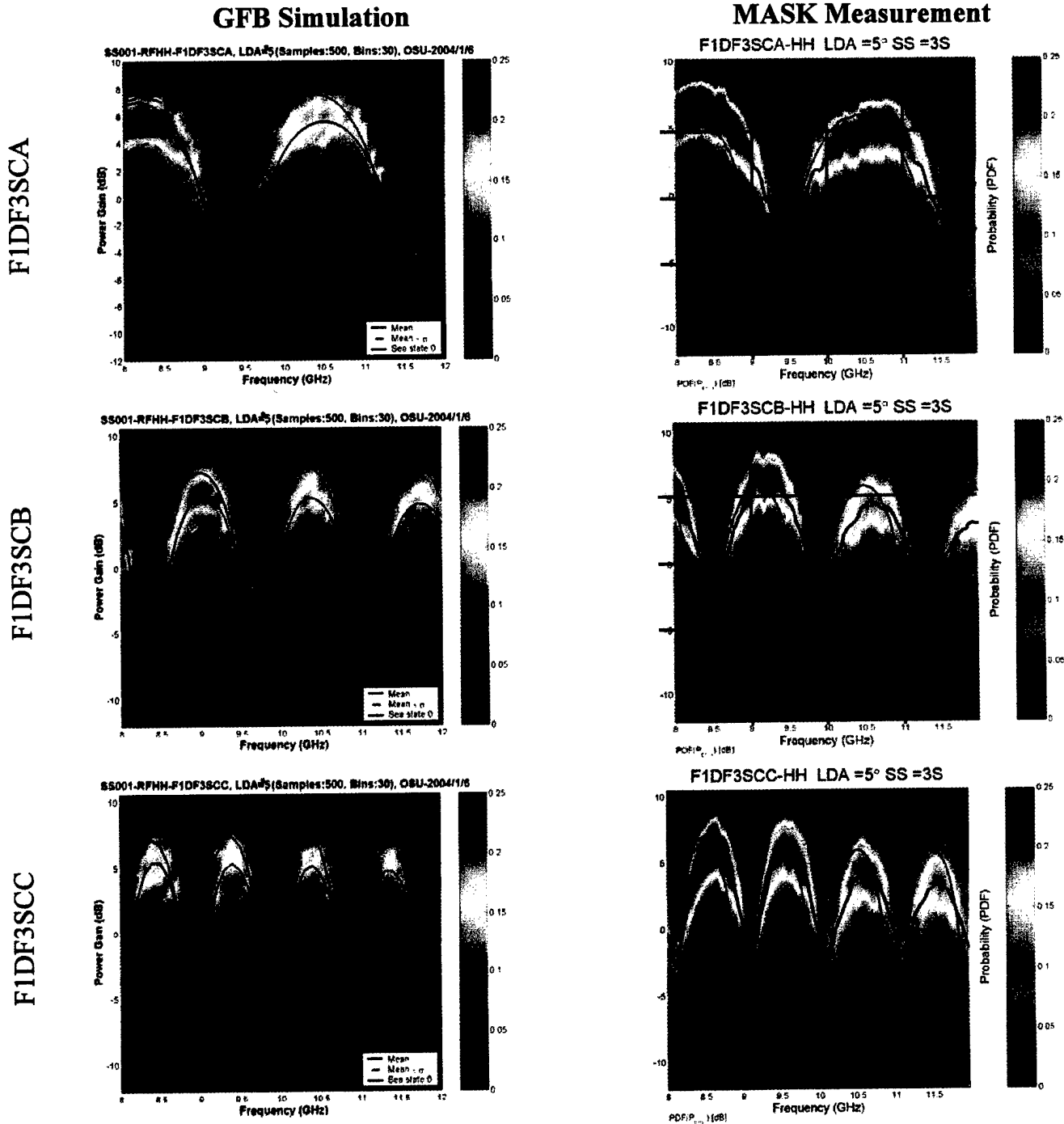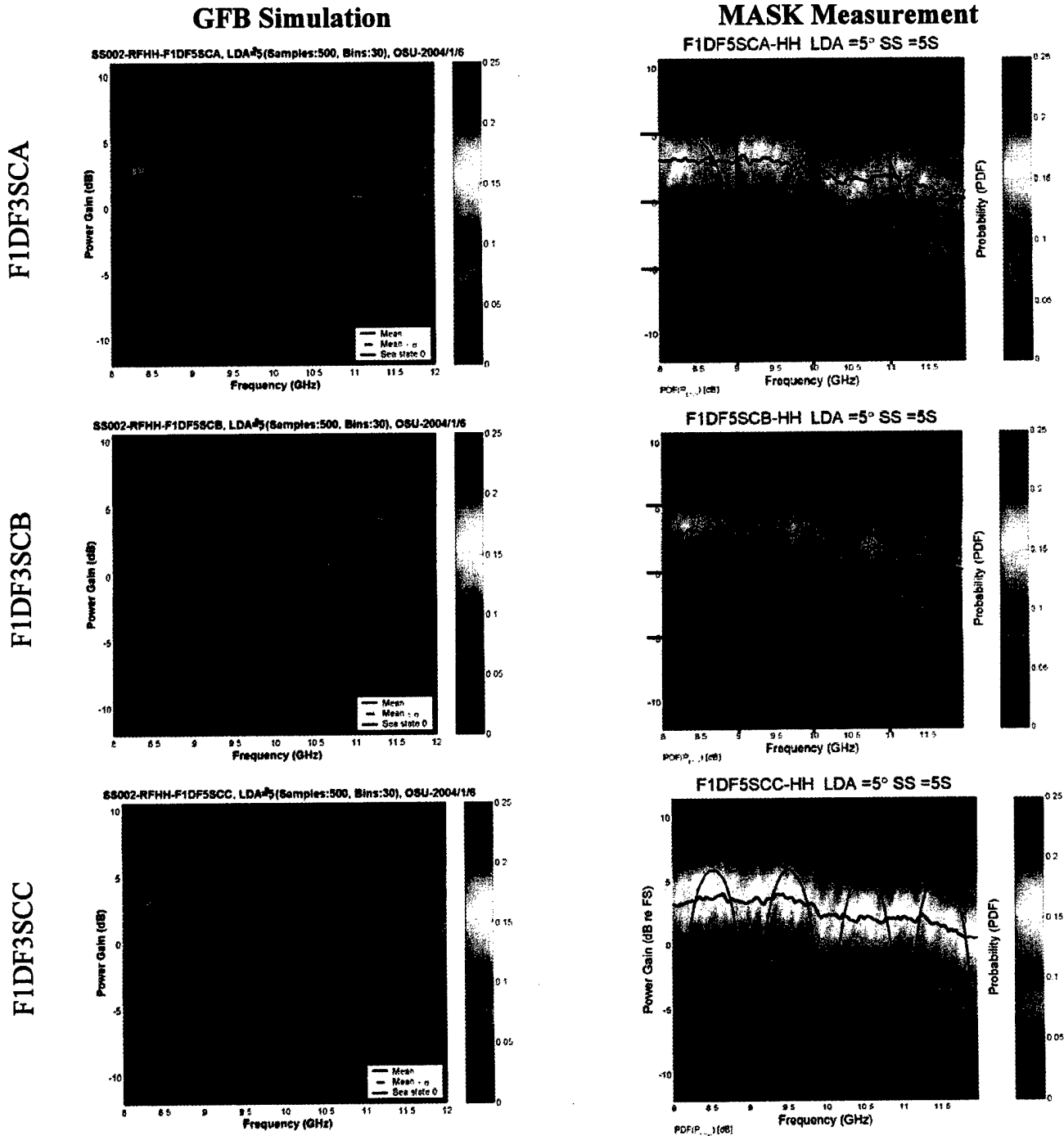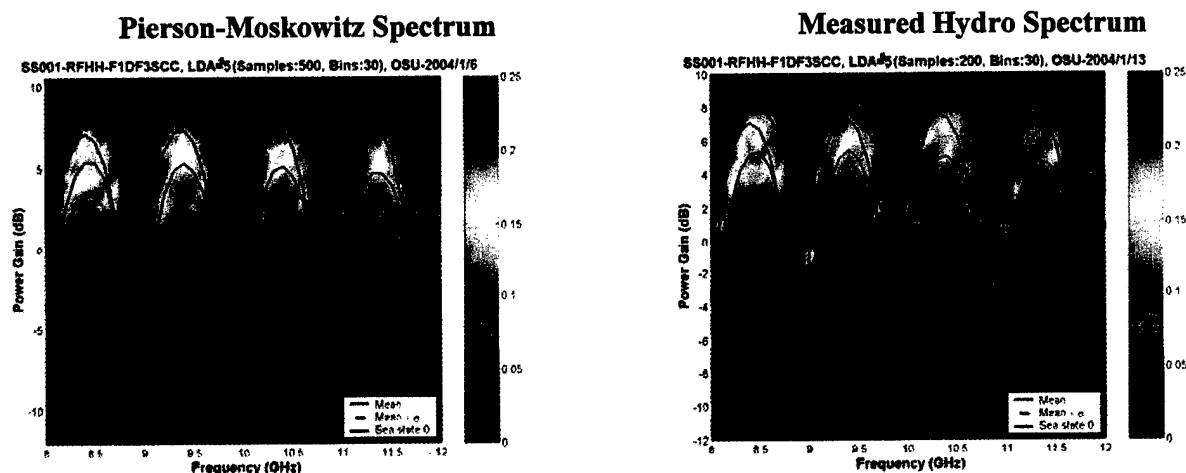**Figure 3.15:** Comparison between simulation and measurements for forward scatter simulation from rough sea surface.

21

3.7 Vertical Polarization Simulations

The simulation setup is shown in Figure 3.16. Transmitter is located at 5.25m with –9.9° and receiver at 1.75m with –3° depression angle. The receiver is at a horizontal range of 60m from the transmitter. Both antennas are vertically polarized. Monte Carlo simulations are performed for sea state 3 and 5 and numerical PDF are plotted against frequency range 8-12 GHz, shown in Figure 3.17 and 3.18.
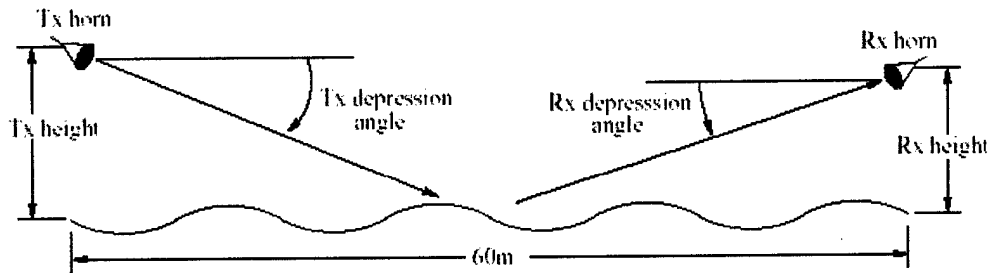
Figure 3.16: Experimental setup for forward scatter measurements over rough sea surface.

SS001-RFVV-F1DF3SCC, LDA=5 (Samples:500, Bins:10), OSU-2004/1/6		
Test	FwdSct
Data Set	F1DF3SCC
Run Name	SS001
Polarization	VV
Sea State	3
Range	60m
Transmitter	-9.9^0 @ 5.25m
Receiver	-3^0 @ 1.75m
LDA	5^0
Samples	500
PDF Bins	10
Organization	OSU
Date	2004/1/6
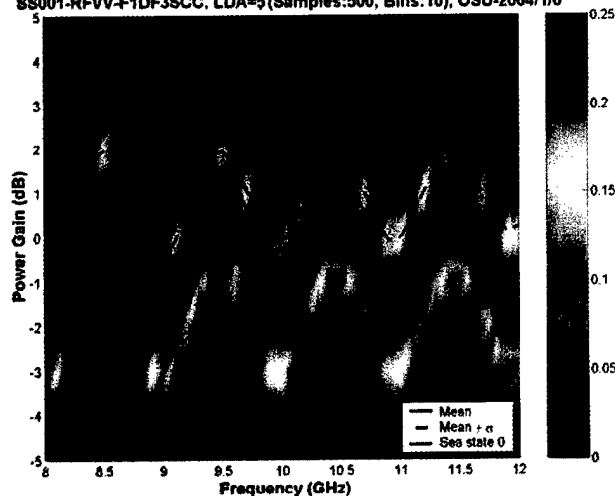
Figure 3.17: Forward scatter probability density function (PDF) for sea state 5, vertical polarization, Tx height = 5.25m, Rx height = 1.75m.

SS002-RFVV-F1DF5SCC, LDA=5 (Samples:500, Bins:10), OSU-2004/1/6		
Test	FwdSct
Data Set	F1DF5SCC
Run Name	SS002
Polarization	VV
Sea State	5
Range	60m
Transmitter	-9.9^0 @ 5.25m
Receiver	-3^0 @ 1.75m
LDA	5^0
Samples	500
PDF Bins	10
Organization	OSU
Date	2004/1/6
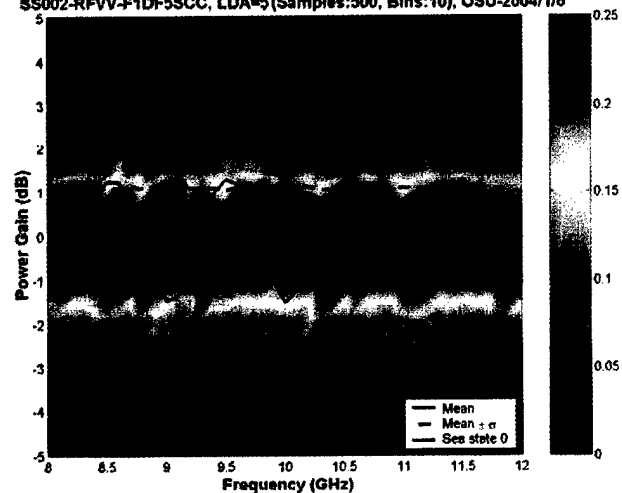
Figure 3.18: Forward scatter probability density function (PDF) for sea state 5, vertical polarization, Tx height = 5.25m, Rx height = 1.75m.

23

3.8 Long bank simulations

For these simulations, we are using long bank (cross wind) instead of short (down wind), as shown in Figure 3.19. The water waves are traveling normal to the line of sight direction between transmitter and receiver. The transmitter is 5.25m high with $-9.9°$ depression angle and the receiver is located at position C ($-3°$ at 1.75m). The range between them is the same as before, i.e., 60m. Sea state 5 is used with both horizontally and vertically polarized antennas. Physical Optics with adaptive sampling technique is employed to compute 100 samples in a Monte Carlo run. The numeric PDF is shown against frequency in Figure 3.20 and 3.21.

Tx
$-9°$ @ 5.25m

Rx
$-3°$ @ 1.75m
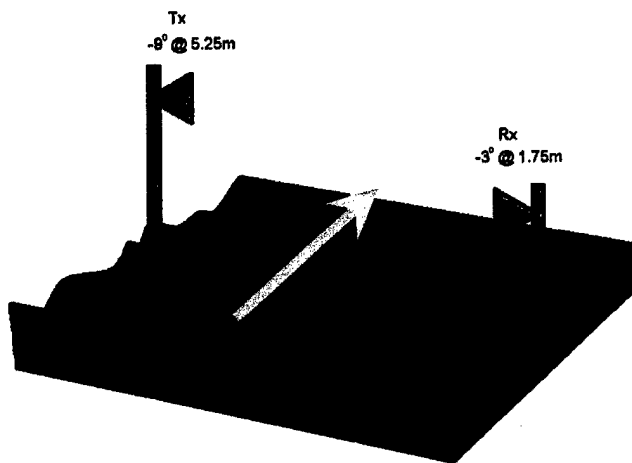
Figure 3.19: Experimental setup for forward scatter measurements over rough sea surface, long bank.

The forward scattering over long bank waves can give rise to "channeling events" where the sea scattering is significantly higher than the incident field. This occurs when a trough passes between the transmit and receive horns in such a way as to focus the reflected field, much like a parabolic reflector. This phenomenon is described in more detail in [13].
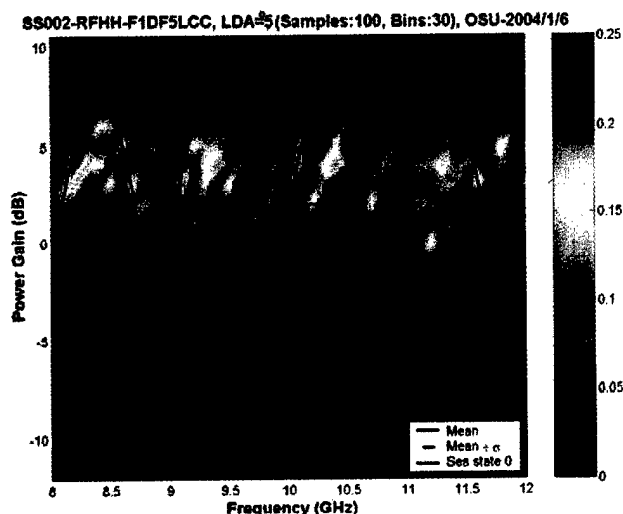
24

SS002-RFHH-F1DF5LCC, LDA=5(Samples:100, Bins:30), OSU-2004/1/6

Test	FwdSct
Data Set	F1DF5LCC
Run Name	SS002
Polarization	HH
Sea State	5
Range	60m
Transmitter	-9.9^0 @ 5.25m
Receiver	-3^0 @ 1.75m
LDA	5^0
Samples	100
PDF Bins	10
Organization	OSU
Date	2004/1/6

Figure 3.20: Forward scatter probability density function (PDF) for sea state 5, long bank, vertical polarization, Tx height = 5.25m, Rx height = 1.75m.

SS002-RFVV-F1DF5LCC, LDA=5(Samples:100, Bins:10), OSU-2004/1/6
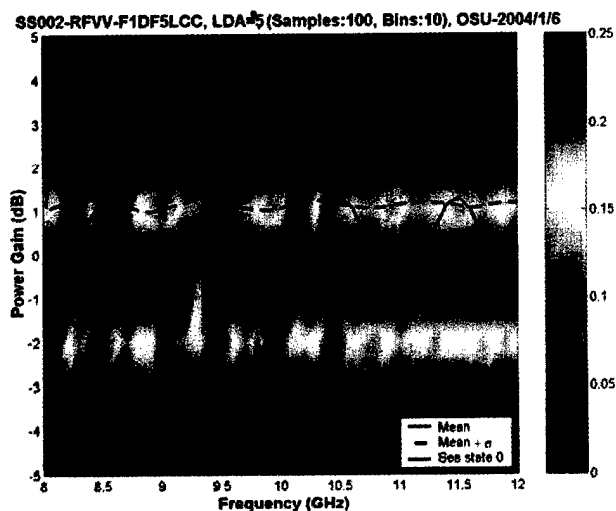
Test	FwdSct
Data Set	F1DF5LCC
Run Name	SS002
Polarization	VV
Sea State	5
Range	60m
Transmitter	-9.9^0 @ 5.25m
Receiver	-3^0 @ 1.75m
LDA	5^0
Samples	100
PDF Bins	10
Organization	OSU
Date	2004/1/6

Figure 3.21: Forward scatter probability density function (PDF) for sea state 5, long bank, vertical polarization, Tx height = 5.25m, Rx height = 1.75m.

25

Chapter 4

Backscatter Simulations

The backscatter experimental setup is shown in Figure 4.1. A transmit/receive horizontally polarized horn antenna is placed 3.14m high with -6° depression angle and illuminates a target at a range of 29.3m over the rough sea surface. The target in this case is a circular cylinder 12 inches high and 17 inches in diameter. Sea states 3 and 5 are investigated. Two cases are considered: floating and non-floating target. A floating target rolls with the waves and is assumed to have zero inertia i.e., free-floating on the water waves. A non-floating target is placed on the surface but does not roll with the waves, although it may move up and down with the waves. In each case, 512 samples are computed in a Monte Carlo run using random rough sea surfaces generated with the Pierson-Moskowitz spectrum.
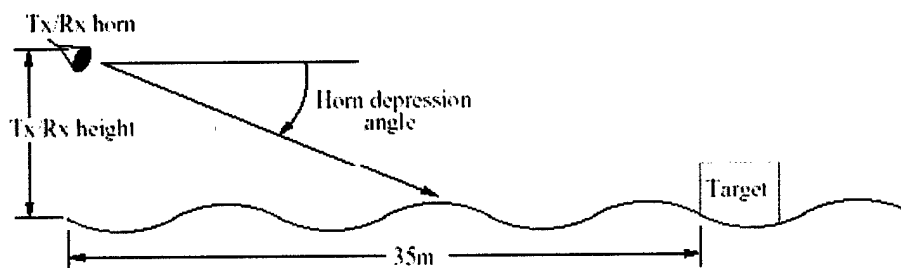
Figure 4.1: Experimental setup for backscatter measurements from a non-floating target over rough sea surface

Figures 4.2 and 4.3 show the PDFs of the floating and non-floating cylinder targets, respectively, for sea state 3, and Figures 4.4 and 4.5 show the same results for sea state 5. The solid red line in each plot is the sea state 0 (flat surface) result for reference. All of these results show that the rough surface significantly lowers the mean backscatter with respect to the flat surface. The comparisons between the floating and non-floating PDFs show that the floating target has about the same mean as the non-floating target, but a larger variance as one might expect.
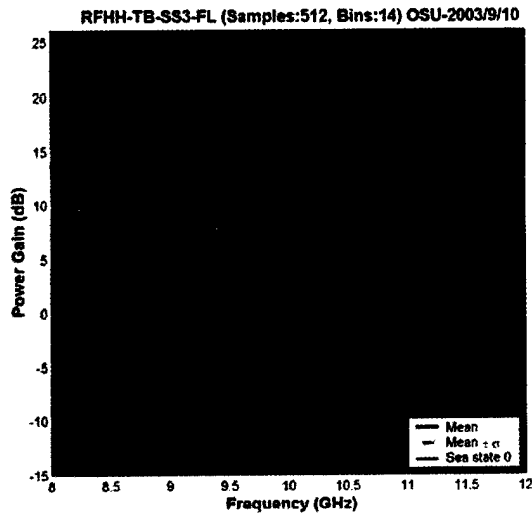
26

Figure 4.2: Backscatter probability density function (PDF) for sea state 3, floating cylinder, horizontal polarization.
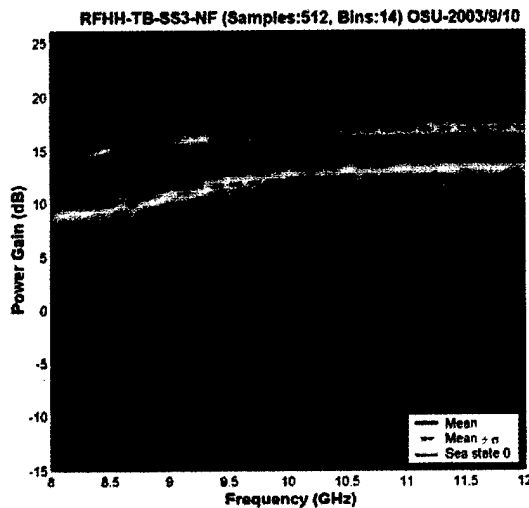
Figure 4.3: Backscatter probability density function (PDF) for sea state 3, non-floating cylinder, horizontal polarization.

27

Figure 4.4: Backscatter probability density function (PDF) for sea state 5, floating cylinder, horizontal polarization.

Figure 4.5: Backscatter probability density function (PDF) for sea state 5, non-floating cylinder, horizontal polarization.

Chapter 5

Radar Cross Section Computation using Hybrid Decoupled Approach

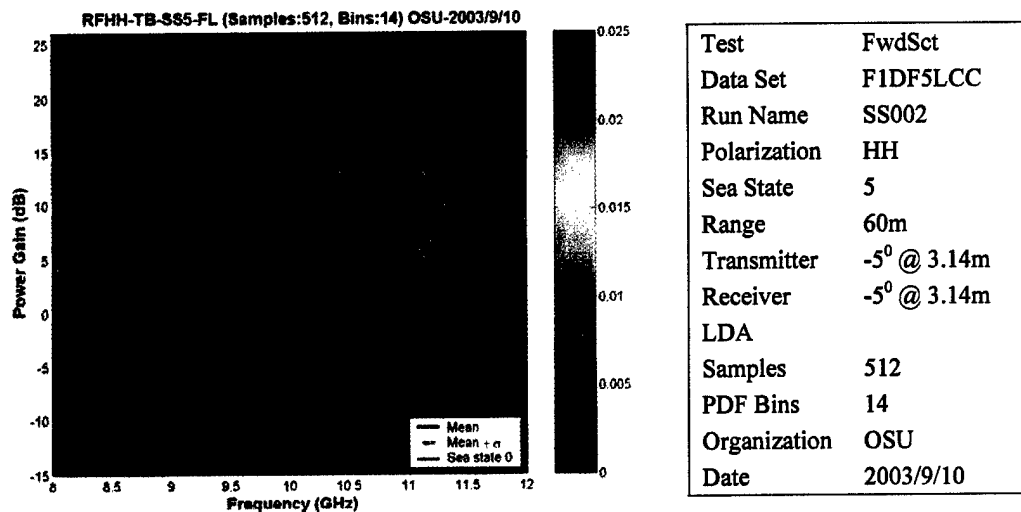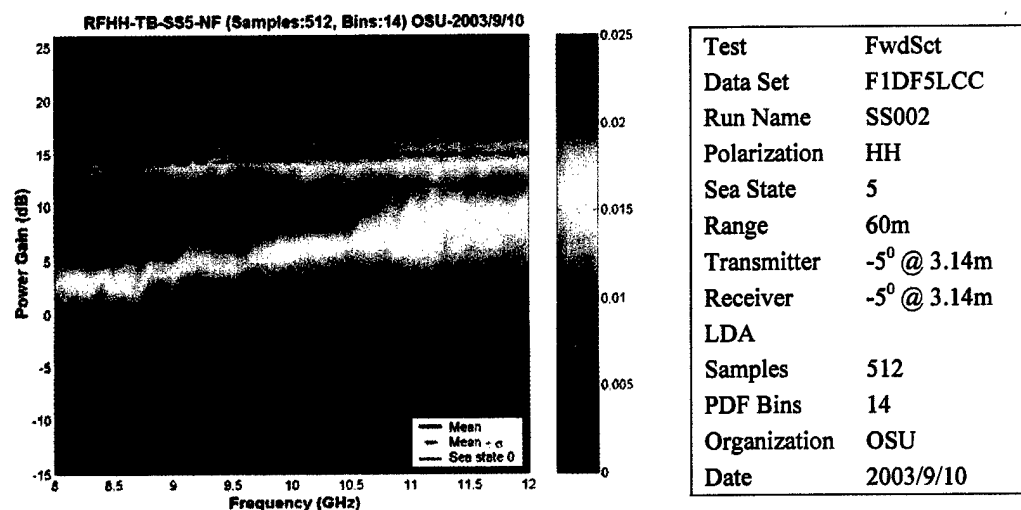## 5.1 Introduction

The prediction of radar cross-section from a realistically large and complex target like ship on a rough sea surface is very challenging. Numerical methods such as the generalized forward-backward method [14] must model the target plus a large portion of the sea surface. This makes the computational domain extremely large, and becomes intractable for 3D targets at radar frequencies. As we know, efficient numerical methods have been well developed to compute the scattering from rough surfaces, such as the canonical grid method [15], physical optics [16,17], iterative physical optics [18], and the non-local small slope approximation [19]. Similarly, efficient numerical solutions are available for complex targets, such as the fast multipole method [20]. In this chapter, we present the idea of decoupling the problem of a large sea surface from the local target problem. The formulation is based upon the reciprocity theorem, and was presented originally in [1].

5.2 Reciprocity Formulation for Backscatter Field

The composite scattering problem is shown in Figure 5.1(a) where an incident field from a source is illuminating a ship-like target in the presence of a rough sea surface. Here, the total fields are defined as incident plus scattered fields,

$$(\overline{E}, \overline{H}) = (\overline{E}_i, \overline{H}_i) + (\overline{E}_s, \overline{H}_s) \tag{5.1}$$

The incident fields are defined as the fields over the sea surface in the absence of the ship as shown in Figure 5.1(b). The scattered fields (E_s, H_s) are defined as total fields minus the incident fields, and are hence the scattering due to the presence of the target on the

sea surface. The volume of space V where the fields of interest exist is bounded by the target surface S_T, the sea surface S_{sea} and the surface at infinity S_∞ above the sea surface.

$$(E,H) = (E_i,H_i) + (E_s,H_s)$$
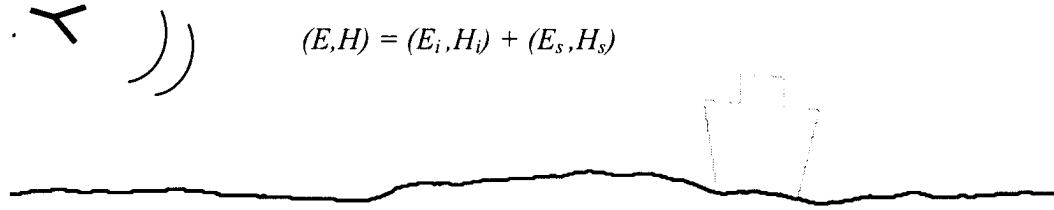
(a) Composite scattering problem of interest.

$$(E_i,H_i)$$
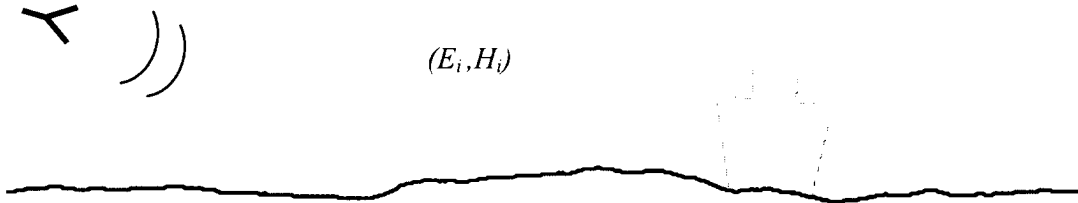
(b) Incident fields without target.

$$(E_t,H_t)$$
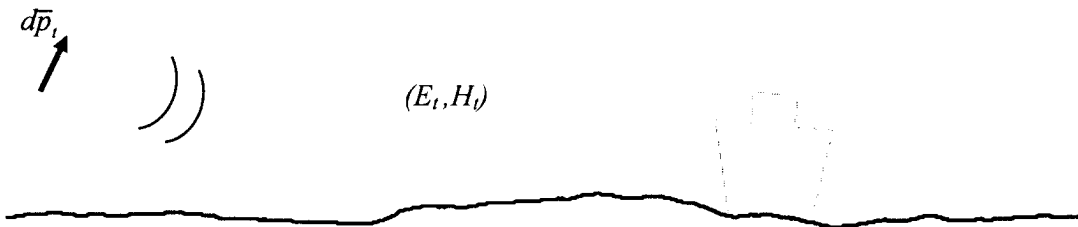
(c) Fields of a test source without target.

Figure 5.1: Sea surface and scattering configurations for the reciprocity formulation. (a) Incident and scattered fields with target present. (b) Incident fields with target absent. (c) Fields of a test source with target absent.

Figure 5.1(c) shows a test case for the application of the reciprocity theorem. An electric point dipole test source dp_t is placed at any point P_t where the scattered field is to be computed. (For backscatter, the test source would be placed at the same location as the original source.) Fields generated by this test source in the presence of the sea surface but in the absence of the target are defined as test fields (E_t, H_t). We apply reciprocity to the test fields and scattered fields over the entire volume V, resulting in the *reaction integral*

$$d\overline{p}_t \cdot \overline{E}_s(P_t) = \int_{S_{sea}+S_\infty+S_T} (\overline{E}_s \times \overline{H}_t - \overline{E}_t \times \overline{H}_s) \cdot \hat{n} \; dS \qquad (5.2)$$

where $\hat{n}$ points into V. Since the test fields and scattered fields satisfy the same boundary conditions on S_{sea} and S_∞, the reaction integral will vanish there yielding the integration over the target surface S_T only,

$$d\overline{p}_t \cdot \overline{E}_s(P_t) = \int_{S_T} (\overline{E}_s \times \overline{H}_t - \overline{E}_t \times \overline{H}_s) \cdot \hat{n} \; dS \qquad (5.3)$$

The above equation is an important result for computational purposes for what it states that the scattered field at a point P_t can be found by finding the incident and scattered fields over the target surface only. This reduces the computational domain significantly from the whole sea surface to target surface only. The scattering from the target can be found in a simple 3-step, semi-decoupled procedure:

1. Find the incident fields (E_i, H_i) and the test fields (E_t, H_t) over S_T with the target absent. (These are the same fields for the case of backscatter.)
2. Find the scattered fields (E_s, H_s) over S_T using the incident fields (E_i, H_i) as excitation.
3. Find the scattered electric field at the point P_t using Eq. (5.3).

This procedure is semi-decoupled because the scattered fields in step 2 are found in the presence of the rough surface. However, only the local rough surface is needed and not the entire sea surface S_{sea}. Furthermore, if a first-order method such as physical optics (PO) or the physical theory of diffraction (PTD) is used to compute (E_s, H_s) then the higher order interactions with the rough surface may be ignored to a good approximation.

Eq. (5.3) may be simplified for a source and receiver at infinity, i.e., for plane wave incidence and far-zone scattering. Replacing the test source with a unit amplitude electric point dipole $\hat{p}$ placed at infinity, the reciprocity equation then becomes,

$$\hat{p} \cdot \overline{E}_s(P_t) = \lim_{r \to \infty} -\frac{jkZ_o}{4\pi} \frac{e^{-jkr}}{r} \int_{S_T} (\overline{E}_s \times \overline{H}_t - \overline{E}_t \times \overline{H}_s) \cdot \hat{n} \; dS \qquad (5.5)$$

where r is the far-zone distance. The expression in (5.5) is an exact formulation for the scattering from a 3-D target derived from Maxwell's equation and boundary conditions on sea surface and at infinity. This equation can be used directly for backscatter and bistatic RCS computations.

31

5.3 Backscatter RCS of a 2D PEC Target

For a perfect electrically conducting (PEC) target, the equivalent electric surface current is defined as

$$\overline{J}_s = \hat{n} \times \overline{H} \tag{5.6}$$

where H is the total magnetic field. Enforcing the PEC boundary condition on S_T, the integrand of equation (5.5) reduces to,

$$
\begin{aligned}
(\overline{E}_s \times \overline{H}_t - \overline{E}_t \times \overline{H}_s) \cdot \hat{n} &= [(\overline{E} - \overline{E}_i) \times \overline{H}_t - \overline{E}_t \times (\overline{H} - \overline{H}_t)] \cdot \hat{n} \\
&= -\overline{E}_t \times \overline{H} \cdot \hat{n} \\
&= \overline{E}_t \cdot \overline{J}_s
\end{aligned} \tag{5.7}
$$

For Backscattering, $(E_t, H_t) = (E_i, H_i)$. Also, using a 2D line current (or line dipole current) as a test source in place of a 3D dipole, the expression in equation (5.5) can be simplified as

$$\hat{p} \cdot \overline{E}_s (P_t) = \lim_{r \to \infty} -Z_o \sqrt{\frac{jk}{8\pi}} \frac{e^{-jkr}}{\sqrt{r}} \int_{S_T} \overline{E}_i \cdot \overline{J}_s \, dS \tag{5.8}$$

The problem is to find the equivalent surface currents on the target surface in the presence of the sea surface where the Green's function for the sea surface is unknown. The backscatter 2D RCS is defined as,

$$RCS_{2D} = \lim_{r \to \infty} 2\pi r |E_s(\overline{r})|^2 \tag{5.9}$$

Using the expression in equation (5.8), it can be given as,

$$RCS_{2D} = \frac{kZ_o^2}{4} \left| \int_{S_T} \overline{E}_i \cdot \overline{J}_s \, dS \right|^2 \tag{5.10}$$

5.4 Numerical Results

To compute the monostatic RCS of a 2D target from equation (5.10), two quantities need to be found:

1. Incident fields in the presence of rough surface but in the absence of the target itself. This quantity can be found exactly by applying integral equation (IE) methods such as the method of moment (MM) with an efficient numerical solver. In this case, we are using the forward-backward (FB) method with spectral acceleration [7].

2. Equivalent surface current J_s, which depends upon the total field, defined by equation (5.6). This quantity is unknown, as the total fields are unknown. However, a good approximation can be made. Here we are approximating the equivalent currents on the surface of the target using physical optics (PO) as,

$$\bar{J}_s \approx \begin{cases} 2\hat{n} \times \bar{H}_i & \text{lit region} \\ 0 & \text{shadow region} \end{cases} \tag{5.11}$$

Following are plots of monostatic RCS vs. incidence (elevation) angle for different targets over a random rough sea surface. The generalized forward-backward (GFB) method is used as a reference solution, and is compared with the hybrid forward-backward method/physical optics (FB/PO) technique.

Figure 5.2 shows the RCS patterns of a vertical flat plate on a flat sea surface. The flat plate forms a corner reflector with the sea surface, so the RCS pattern is expected to be very high for most incidence angles. The GFB and hybrid FB/PO reciprocity results are shown on this plot, along with a reference solution found using the Green's function for an infinite flat surface. The results are in good agreement. At low grazing angles, some differences can be seen due to the finite length of the sea surface used in the GFB and FB/PO computations.
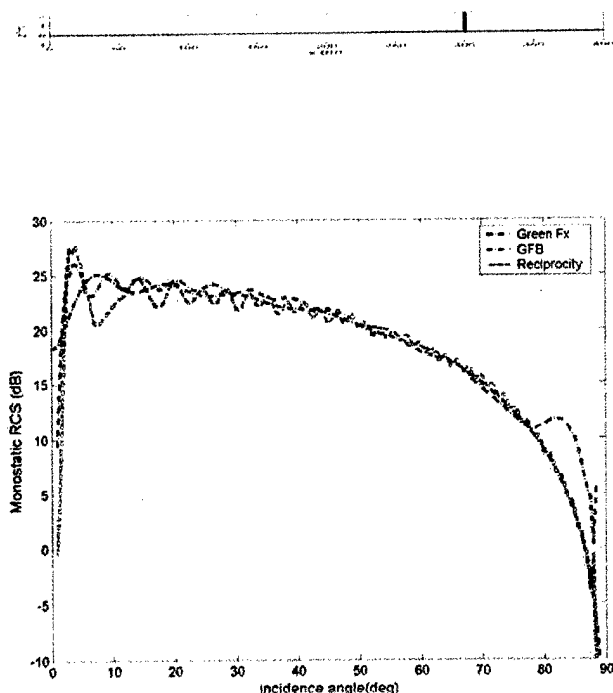

Figure 5.2: Backscatter from a 2m vertical plate on flat sea surface (sea state 0) computed using GFB and hybrid method using reciprocity. Frequency is 1 GHz, horizontal polarization.

33

Figure 5.3 shows the RCS patterns of a vertical flat plate on a rough sea surface at sea state 3. The agreement between the GFB reference solution and the hybrid reciprocity approach is very good. In these results the total field is plotted, rather than just the target scattered field, so the RCS becomes dominated by the surface scattering as the incidence angle approaches 90 degrees. At low grazing angles the RCS is dominated by the plate and plate-surface interaction.
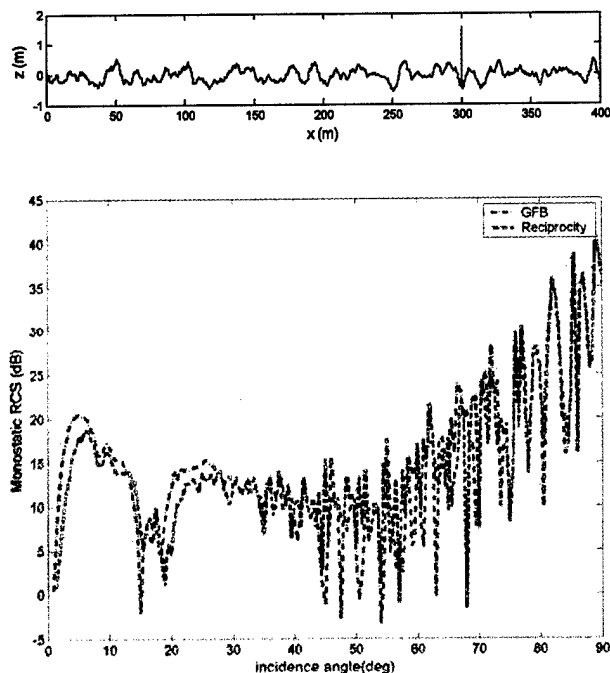

Figure 5.3: Backscatter from a 2m vertical plate on rough sea surface (sea state 3) computed using GFB and hybrid method using reciprocity. Frequency is 1 GHz, horizontal polarization.

34

Figure 5.4 shows the RCS patterns of a floating block target. Again, the total scattering is plotted so the surface scattering dominates at high angles of incidence. These patterns are under-sampled, so they appear less smooth.
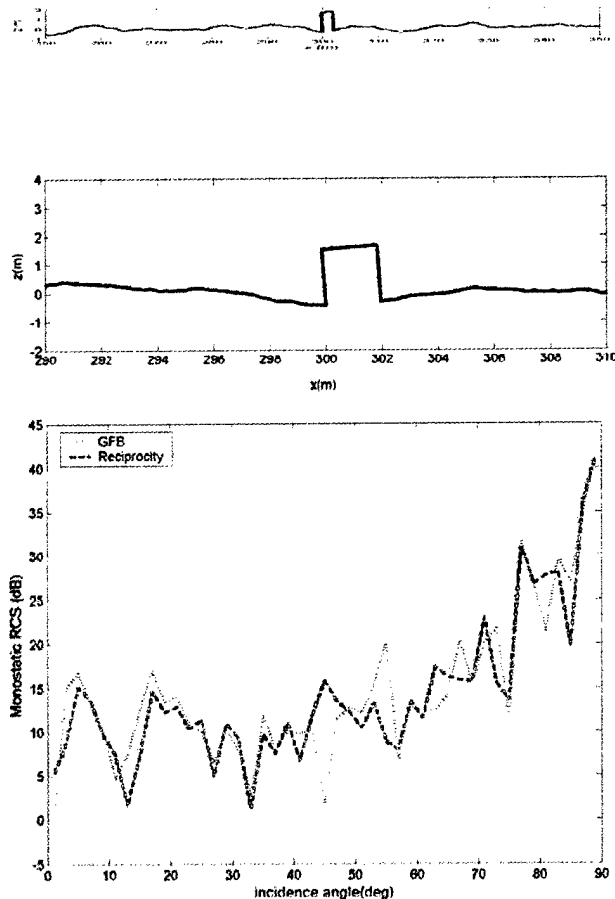

Figure 5.4: Backscatter from a 2m x 1m block on a rough sea surface (sea state 3) computed using GFB and hybrid method using reciprocity. Frequency is 1 GHz, horizontal polarization.

35

Figure 5.5 shows the RCS patterns of a low-observable target on a rough surface. The total scattering is plotted. The agreement between the GFB reference solution and the hybrid FB/PO/reciprocity solution is very good. The peak at 20 degrees is where the incident field is broadside to the slanted side of the target.
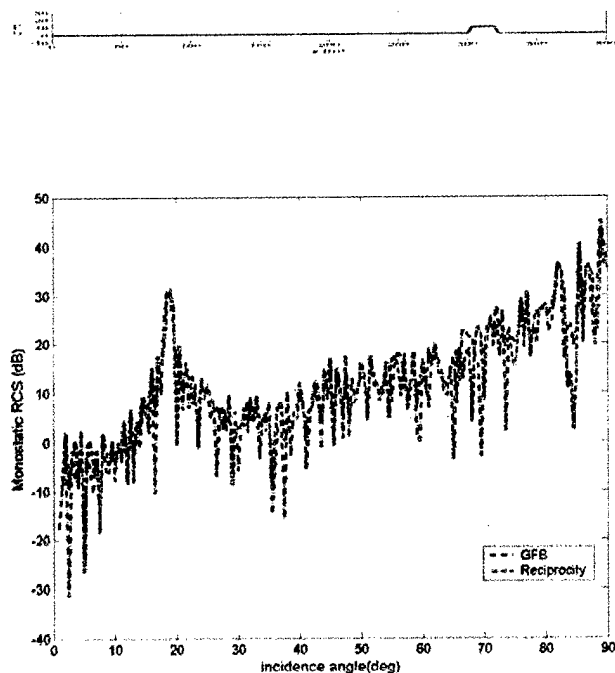

Figure 5.5: Backscatter from a low-observable target on a rough sea surface (sea state 3) computed using GFB and hybrid method using reciprocity. Frequency is 1 GHz, horizontal polarization. Target is 9m high and 20m across at the base, with 20 degree angled sides.

Chapter 6 Conclusions

The comparisons of the numerical simulations with the measured data from simulation sets SS001 and SS002 of Chapter 3 are generally very good. This validates the accuracy of the GFB code. Some discrepancies were observed, such as the pronounced downward trend of the mean forward scattering with frequency in the measurements. A simulation was run using the measured sea spectrum to rule out the possibility that the discrepancies are caused by using the Pierson-Moskowitz spectrum in the GFB code. It was found that the spectrum was not the cause. Most likely the discrepancies are due to the 2D model. It is known that the incoherent scattering from a rough surface is proportional to the spot size illuminated by the incident radar beam. This spot size varies with frequency due to the frequency dependence of the horn pattern. The 2D model should accurately include the length variation of the spot size, but not the width variation in the third dimension. The width of the spot is expected to decrease with frequency, and hence, the incoherent scattering should also decrease. This would explain the more pronounced downward trend observed in the measurements. Re-simulations of sets SS001 and SS002 will attempt to include the width variation of the spot size.

The backscatter simulations of floating and non-floating targets in Chapter 4 yielded insight into the RCS variations that one would expect when a floating target rolls on a sea surface. The RCS of a free-floating target is observed to have about the same mean, but much larger variation compared with a floating target that does not roll with the waves. To the authors' knowledge, this is the first time that the scattering from a free-floating target on the sea has been rigorously modeled.

Chapter 5 presented the first results of a decoupled approach to computing the scattering from targets on a rough surface. This hybrid decomposition combined the forward-backward method for the sea surface with physical optics for the target, using a reciprocity formulation to compute the composite scattering. Good agreement is found between this new approach and the GFB reference solution. In the future, more accurate techniques will be applied to the target region, such as the physical theory of diffraction (PTD), unified theory of diffraction (UTD) or the fast multipole method (FMM). The method will also be extended to 3D using 3D rough surface scattering predictions such as the sparse matrix canonical grid method and the non-local small slope approximation.

References

[1] R.J. Burkholder, M.R. Pino, and D.-H. Kwon, "Development of Ray Optical Methods for Studying the RCS of 2D Targets on a Rough Sea Surface," The Ohio State University ElectroScience Laboratory Technical Report 735231-1, January 1999.

[2] R.J. Burkholder, D. Colak, and H. Kiper, "Numerical Investigation of the RCS of 3D Targets on a Rough Sea Surface," The Ohio State University ElectroScience Laboratory Technical Report 735231-2, January 2000.

[3] R.J. Burkholder, P. Janpugdee, and D. Colak, "Development of Computational Tools for Predicting the Radar Scattering from Targets on a Rough Sea Surface," The Ohio State University ElectroScience Laboratory Final Report 735231-3, January 2001.

[4] R.J. Burkholder, and Khalid Jamil, "Simulation of Electromagnetic Scattering Experiments in the NSWC Carderock MASK Facility," The Ohio State University ElectroScience Laboratory Final Report 742962-1, February 2003.

[5] D. Holliday, L.L. DeRaad, and G.J. St-Cyr, "Forward-Backward: A new method for computing low-grazing angle scattering," IEEE Trans. Antennas and Propagation. Vol. 44, pp. 722-729, May 1996.

[6] P. Tran., "Calculation of the scattering electromagnetic waves from a two-dimensional perfectly conducting surface using the method of ordered multiple interactions," *Waves in Random Media,* vol. 7, no. 3, pp. 295-302, July 1997.

[7] H.-T. Chou and J.T. Johnson, "Novel Acceleration algorithm for Forward-Backward method in the computation of scattering from rough surfaces," *Radio Science,* vol. 33, no. 5, pp. 1277-1287, 1998.

[8] M.R. Pino and F. Obelleiro, and R.J. Burkholder, "Spectral Acceleration of the Generalized Forward-Backward Method," *IEEE Trans. On Antennas and Propagation,* Vol. 50, No. 6, pp.785-797, June 2002.

[9] W. J. Pierson and L. Moskowitz, "A proposed spectral form for fully developed wind seas based on the similarity theory of S.A.Kitaigorodskii," *J. Geophysics Res.,* vol. 69, pp. 5181-5190, 1964.